PHYSICAL REVIEW E, VOLUME 65, 045401(R)

Perturbation transfer from the front to rear surface of laser-irradiated targets

K. Shigemori,[1] H. Azechi,[1] M. Nakai,[1] T. Endo,[1,2] T. Nagaya,[1] and T. Yamanaka
[1]*Institute of Laser Engineering, Osaka University, Suita, Osaka, 565-0871, Japan*
[2]*Center for Integrated Research in Science and Engineering, Nagoya University, Nagoya, 464-8603, Japan*
(Received 12 October 2001; published 10 April 2002)

We present experimental results on the perturbation transfer of laser irradiated planar foils. Perturbed polystyrene foils were irradiated directly by laser at intensity of 6×10^{13} W/cm^2. We measured perturbations on the foils by side-on x-ray backlighting technique. Perturbations on the rear surface due to the rippled shock front were observed just after the shock breakout. We also observed feedthrough of perturbations on the laser-irradiated surface that grows due to the Rayleigh-Taylor instability.

DOI: 10.1103/PhysRevE.65.045401 PACS number(s): 52.50.Jm, 52.35.Tc, 52.70.La

It is well known that hydrodynamic instabilities are crucial for better understanding of inertial confinement fusion (ICF) targets [1]. The hydrodynamic instabilities are also important in astrophysical plasmas, such as supernovae explosions [2]. The most crucial hydrodynamic instability in ICF targets is the Rayleigh-Taylor (RT) instability [3,4] that occurs both on the laser-irradiated surface and the rear surface. Perturbations on the laser-irradiated surface of the ICF targets grow due to the RT instability when the target shell accelerates inward. On the other hand, perturbations on the rear surface grow due to the RT instability when the target shell decelerates after the reflecting shock wave reaches the rear surface. The Richtmyer-Meshkov (RM) instability [5] that is one variety of the RT instability also takes place when the shock wave passes through interfaces of the laser-irradiated surface and the rear surface, which should be a possible seed of the RT instability. Since the criteria of the ignition of the ICF targets is determined by the perturbations of the compressed central fuel (the hot spark) at around the maximum compression, it is important to understand the perturbation transfer from front to rear side of the main fuel. However, to date, most investigations of the hydrodynamic instability have been focused on the laser-irradiated surface except for a few experiments [6–8].

When an ICF target is irradiated by a laser pulse, a shock passes through the shell target. If the laser-irradiated surface is perturbed, or if spatial nonuniformity are imposed on the laser pulse, the shock front should be rippled [9]. The rear surface is deformed due to the passage of the rippled shock front [10], which is called ''feed-in.'' The source of the feed-in of the rear surface perturbation is both from the time difference of the shock breakout between the crest and the trough of the ripped shock front and from the pressure perturbation just behind the rippled shock front, which is very similar to the RM instability described above. On the other hand, perturbation is transferred from the laser-irradiated surface to the rear surface due mainly to the communication through the sound wave that propagate back and forth, which occur when the target is accelerated. This phenomena is called ''feed-through.''

In this paper, we describe the experiments about the feed-in and the feed-through of laser-irradiated targets. We observed the feed-in perturbation due to the rippled shock front breakout at the rear surface of the target. The feed-through perturbations were also clearly observed when the laser-irradiated foils were accelerated. We calculated the perturbation amplitude due to the feed-in and the feed-through by a simple model coupled with a one-dimensional (1D) hydrodynamic simulation code, which shows good agreement with the experimental results.

The experiments we describe here were carried out on the GEKKO XII laser system at the Institute of Laser Engineering, Osaka University [11]. Targets with initial perturbations were directly irradiated by laser. Since it is very important to irradiate the targets with a spatially uniform laser, we employed partially coherent light (PCL) [12] as the driving laser. We furthermore employed random phase plates [13] to get a smoother irradiation pattern. The nonuniformity of the laser beam was approximately 2.4% from a smooth envelope. The pulse duration of the PCL was 2.3 ns in full width at half maximum. The rise time and the decay time of the pulse were 50 ps and 150 ps, respectively. The laser energy of each PCL beam was approximately 350 J (2ω). Two PCL beams were focused on the target with a spot diameter of ≈600 μm. The incident angle of each laser beam was 37.4 deg. The intensity on the target was 6×10^{13} W/cm^2.

The irradiated targets were polystyrene (CH) foils ($\rho=1.056$ g/cm^3). The thickness of the foil was 16 μm or 25 μm. We imposed perturbations on one side of the foil with thermal press technique. The perturbation wavelengths were 60 and 100 μm with the initial peak-to-valley amplitudes of 6 and 10 μm, respectively, which is 10% of the perturbation wavelength. For the side-on x-ray backlighting measurements, we restricted the target width to 200–250 μm to avoid the effect of the target bowing and other issues.

We employed an x-ray framing camera (XFC) in side-on x-ray backlighting geometry to obtain two-dimensional images of the perturbation on the foils. Copper (Cu) backlight targets were irradiated by a beam of the PCL with laser intensity of $\approx4\times10^{13}$ W/cm^2. Beryllium foils of 10-μm thickness was located between the perturbed CH foils and the backlight target to prevent the CH foil from heating with soft x rays from the backlight target. The backlit perturbations on the target were imaged by two pinholes with a 10-μm diameter onto gold photocathodes of the XFC. The diameter of the pinholes was 10 μm. The magnification of the XFC was 30. Temporal resolution of the XFC was

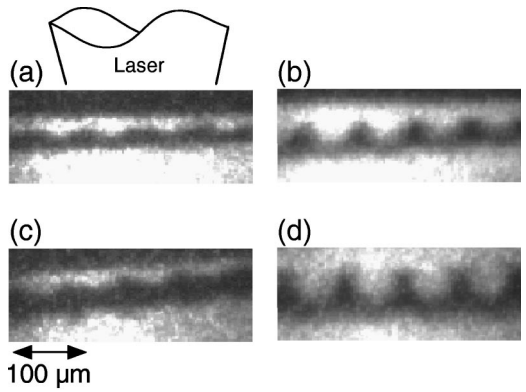

FIG. 1. Examples of the side-on backlit images from the x-ray framing camera at (a) 0.81 ns, (b) 1.31 ns for the 16-μm target, (c) 1.11 ns, and (d) 2.16 ns for 25-μm-thick target.

$\approx$90 ps. The photocathode of the XFC was gold (Au). We obtained two snapshots for each laser shot. The interval of the two snapshots was 500 ps. The x-ray energy of the Cu backlight was 1.1–1.6 keV (L band). Since the width of the target and the rarefaction tail of the CH were 250 μm and $\approx$0.1 g/cm^3, the areal density of the rarefaction tail was $\approx$20 g/cm^2. As the corresponding transmission at the rarefaction tail for the backlit x ray is $<$30%, the observed edge for the rear surface is almost the rarefaction tail.

Figure 1 shows examples of the experimental images from the XFC for 60-μm perturbation wavelength targets. Fig. 1(a) and 1(b) are the images for the 16-μm-thick target at 0.81 ns and at 1.31 ns, respectively. The observation timings shown in Fig. 1 is the time after the half maximum of the rise time of the laser pulse. With the streaked sidelighting, we measured the time at which the shock breaks the rear surface and time at which the rarefaction reaches the front surface to be $\approx$0.9 ns and $\approx$1.34 ns, respectively, for 25-μm thick target [8]. The shock velocity and the rarefaction velocity are $(3.4\pm0.4)\times10^6$ cm/s and $(2.5\pm0.3)\times10^6$ cm/s, respectively. In Fig. 1(a), it is seen that small perturbations arise at the rear surface. In the case of the 16-μm thick target, the shock breakout time and the rarefaction breakout time are expected to be 0.57 ns and 0.86 ns, respectively. Thus at 0.81 ns for the 16-μm-thick target, the shock front has already passed the rear surface, but the target is not accelerated because the rarefaction front has not reached the laser-irradiated surface yet. Thus the rear surface is in the feed-in regime. Figure 1(b) is the image at 1.31 ns for 16-μm-thick target. At 1.31 ns for the 16-μm-thick target, the rarefaction front has already reached the laser-irradiated surface, so the rear surface is in the feed-through regime. It is observed that the perturbations on the rear surface have the same phase as the perturbations on the laser-irradiated surface for both cases. Figures 1(c) and 1(d) are the images for the 25-μm-thick targets at 1.11 ns and 2.16 ns, respectively. At 1.11 ns for the 25-μm-thick target, the rear surface is in the feed-in regime. The rear surface perturbation in Fig. 1(c) shows that the phase was reversed from the initial perturbation of the laser-irradiated surface. At 2.16 ns in Fig. 1(d), the rear surface is in the feed-through regime. The phase of the rear surface perturbation is the same as that of the perturbation of the laser-irradiated surface. This implies that the phase of the perturbation was inverted between 1.11 ns and 2.16 ns.

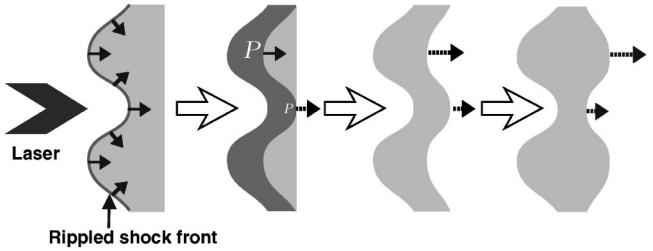

FIG. 2. Schematic mechanism of the feed-in on the rear surface of the laser-irradiated targets.

Now let us calculate the feed-in amplitude of the rear surface perturbation. When laser irradiates a corrugated target surface, a rippled shock launches in accordance with the surface corrugation. The rippled shock propagates in the target with damped oscillation [9] due to the pressure perturbation behind the shock front. The rippled shock front creates perturbations on the rear surface during its transit at the rear surface because the timing of the transit differs due to its spatial perturbation, that is, the crest of rippled shock front reaches the rear surface earlier than the trough of the shock front. Thus at the same time, the pressure perturbation behind the rippled shock front generates velocity perturbation. Figure 2 represents the relation of the rippled shock front oscillation and the feed-in. There is no pressure perturbation behind the shock front immediately after the laser irradiation. Due to the shock convergence, however, the pressure increases at the vicinity of the trough of the shock front. Since the local velocity of the shock front near the trough is faster than that of the crest due to its pressure perturbation, the shock front is flattened. The pressure perturbation becomes maximum when the shock front becomes flat. The pressure perturbation becomes zero again when the inverted shock has the maximum amplitude. When the crest of the shock front reaches the rear surface, the rear surface starts to move as a rarefaction tail, thereby creating a perturbation at the rear surface. The amplitude of the rear surface perturbation increases until the trough of the shock front reaches the rear surface. When the pressure at the shock trough is higher than that at the shock crest, the rarefaction tail of the trough has higher velocity than that of the crest. Therefore the rarefaction tail at the trough catches up and overcomes that of the crest at a certain time.

The time difference of the shock breakout between the crest and the trough is a_s/v_s, where a_s is the peak-to-valley shock amplitude and v_s is the mean shock velocity. The crest of the rarefaction tail moves at a velocity v_r until the trough of the shock front reaches the rear surface, where v_r is the rarefaction tail velocity at the crest. The rarefaction tail of the trough starts to move with velocity of $\sqrt{\alpha}v_r$, where α is the ratio of the pressure at the trough of the shock front to the pressure at the crest of the shock front. The peak-to-valley amplitude of the rear surface is given by

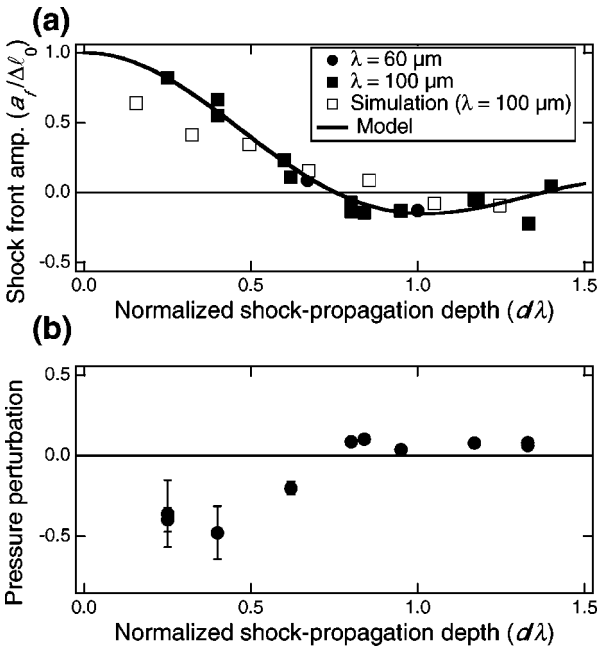

FIG. 3. (a) Rippled shock amplitude normalized by initial amplitude. Negative amplitude means that the ripple is inverted. (b) Normalized pressure perturbation of the rippled shock front. Negative amplitude means that the pressure at the crest of the shock front is smaller than the pressure at the trough of the shock front.

$$a_r = \begin{cases} v_r\left(\dfrac{a_s}{v_s}+\Delta t\right) & \left(-\dfrac{a_s}{v_s}<\Delta t<0\right) \\ a_s\dfrac{v_r}{v_s}+(1-\sqrt{\alpha})v_r\Delta t & (\Delta t>0), \end{cases} \tag{1}$$

where Δt is the time after the trough of the shock front reaches the rear surface. When a_r is negative, the phase of the rear surface perturbation is inverted.

Two parameters in Eq. (1), a_s, α, were obtained from the rippled shock experiments [9,14]. In these experiments, the amplitudes of the rippled shock front a_s were analyzed from optical streaked image of the shock front by the time difference of the shock arrival timing between the crest and the trough of the shock front. The plot of the rippled shock amplitude is shown in Fig. 3(a) [14]. The amplitude of rippled shock front shows damped oscillation. The rippled shock amplitude (a_s) divided by the initial perturbation amplitude appears as a unique function of the shock propagation depth divided by the perturbation wavelength (d/λ). The shock front is flattened at $d/\lambda \approx 0.75$. We also obtained the pressure perturbation from the perturbation of the rear surface emission measured with the optical streak camera. Since the observed energy band (3.1–4.1 eV) of the optical streak camera was much lower than the photon energy that gives the maximum emissivity of blackbody with the simulated temperature of ≈ 5 eV, the observed signal intensity at the shock front is approximately proportional to the temperature. Since the density behind the shock wave is expected to be almost uniform, we may obtain the pressure perturbation from the temperature perturbation via the relation $\delta P/P = \delta T/T$. Figure 3(b) shows analyzed pressure ratio of the rippled shock wave $[P_{\text{crest}}/2(P_{\text{trough}}+P_{\text{crest}})]$. The maximum pressure ratio is ≈ 3 at around $d/\lambda \approx 0.4$. Substituting the pressure ratio α into Eq. (1), we obtained the calculated feed-in amplitude.

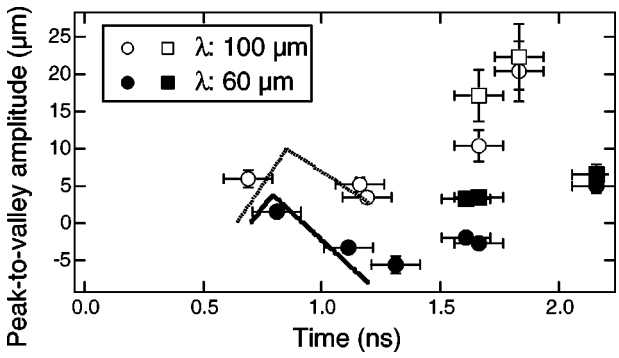

FIG. 4. Observed perturbation amplitude on the rear surface (circles) and calculated feed-through amplitude from the observed laser-irradiated surface amplitude and the target thickness using a simple model (squares). Solid line and dotted line show calculated feed-in amplitudes for 60-μm and 100-μm perturbation wavelength targets, respectively.

Figure 4 shows the measured amplitude of the rear surface perturbation (circles) and the calculated perturbation amplitude from Eq. (1) (lines) for the 25-μm-thick target. The remaining two parameters in Eq. (1), v_r, v_s, are calculated from the 1D hydrodynamic code ILESTA [15]. We experimentally validated these parameters at the same time by the side-on x-ray backlighting measurements with x-ray streak camera [8]. The feed-in perturbation starts to grow when the crest of the shock front reaches the rear surface. After the shock front entirely reaches the rear surface, the amplitude decreases and turns to have the negative value as shown in Fig. 4. This is because the pressure of the crest of the shock front is smaller than the pressure at the trough of the shock front. Since the rarefaction front reaches the laser-irradiated surface at around 1.2 ns, the feed-in regime is from 0.7 to 1.2 ns.

Next we discuss the feed-through of perturbations of the laser-irradiated surface. The feed-through is thought to be an appearance of spatially decaying perturbation on the rear surface. Thus, when the perturbation amplitude is much less than the perturbation wavelength, the rear surface amplitude is given by $a_r = a_f \exp(-kD)$, where k is the wave number of the perturbation, and D is the target thickness. In order to test this simple feed-through model, we calculated the feed-through amplitude from the amplitude on the laser-irradiated surface. The calculated feed-through amplitude from the observed amplitude on the laser-irradiated surface is shown in Fig. 4. Since both sides of the target is deformed due to the RT growth, it is very difficult to determine the target thickness from the experimental images. Instead, we employed the calculated target thickness (D) from the 1D simulation ILESTA, and experimental amplitude on the laser-irradiated surface (a_f). For the 25-μm-thick target, the rarefaction reaches the laser-irradiated surface at 1.2 ns. Thus the feed-through regime is after 1.2 ns for 25-μm target. The calculated feed-through amplitude is in good agreement with the

experimental amplitude in the late time (~ 2 ns). However, there is a significant difference between the calculated amplitude and the experimental amplitude in the earlier time. This is because the perturbations on the laser-irradiated surface are not sufficiently transferred via the sound wave in the earlier timing. Since the sound speed in the accelerated foil is calculated to be $\approx 2\times 10^6$ cm/s, the transit time of sound wave is ≈ 500 ps for the calculated thickness of the foil (≈ 10 μm) after the acceleration. Also, the pressure perturbation still remains in the vicinity of the rear surface. Therefore, the calculated feed-through amplitude must be overestimated. Note that the perturbations on the laser-irradiated surface do not turn into strongly nonlinear growth regime so that a two-dimensional effect should be ruled out. We also observed the feed-through perturbations for the 16-μm-thick targets. But the feed-through perturbations for the 16-μm targets were unclear because the perturbations on the laser-irradiated surface rapidly transform into bubble-spike structure due to its large acceleration.

In conclusion, we have presented the experimental investigation of the perturbation transfer from the front surface to the rear surface in laser-irradiated targets. We observed two types of perturbation transfers: feed-in and feed-through. We calculated the feed-in amplitude by a simple model coupled with the 1D simulation. The feed-in amplitude from the experiments shows good agreement with the model calculation. We also observed feed-through of the perturbation on the laser-irradiated surface, which increases the RT instability. The feed-through perturbation amplitude was exponentially reduced from the amplitude on the laser-irradiated surface as a function of the target thickness and the perturbation wavelength.

The authors gratefully acknowledge the Institute of Laser Engineering, Osaka University. The authors also acknowledge fruitful discussion with Professor K. Nishihara. One of the authors (K.S.) has been supported by the Japan Society for Promotion of Science (JSPS).

[1] J. H. Nuckols *et al.*, Nature (London) **239**, 139 (1972).
[2] T. Shigeyama and K. Nomoto, Astrophys. J. **360**, 242 (1990); W. D. Arnett *et al.*, Astrophys. J. Lett. **341**, L63 (1989).
[3] Lord Rayleigh, *Scientific Papers* (Dover, New York, 1965), Vol. II, p. 200.
[4] G. I. Taylor, Proc. R. Soc. London, Ser. A **201**, 192 (1950).
[5] R. D. Richtmyer, Commun. Pure Appl. Math. **13**, 297 (1960); E. E. Meshkov, Fluid Dyn. **4**, 101 (1969).
[6] W. W. Hsing and N. M. Hoffman, Phys. Rev. Lett. **78**, 3876 (1997); W. W. Hsing *et al.*, Phys. Plasmas **4**, 1832 (1997).
[7] S. T. Weir *et al.*, Phys. Rev. Lett. **80**, 3763 (1998).
[8] K. Shigemori *et al.*, Phys. Rev. Lett. **84**, 5331 (2000).
[9] T. Endo *et al.*, Phys. Rev. Lett. **74**, 3608 (1995); **75**, 2908 (1995).
[10] J. O. Kane *et al.*, Phys. Rev. E **63**, 055401 (2001).
[11] C. Yamanaka, IEEE J. Quantum Electron. **QE-17**, 1639 (1981).
[12] H. Nakano *et al.*, Appl. Phys. Lett. **63**, 580 (1993).
[13] Y. Kato *et al.*, Phys. Rev. Lett. **53**, 1057 (1984).
[14] K. Shigemori *et al.*, Institute of Osaka University Annual Progress Report, 1995 (unpublished).
[15] H. Takabe *et al.*, Phys. Fluids **31**, 2884 (1988).